American Mineralogist, Volume 94, pages 1271–1278, 2009

First-principles energetics and structural relaxation of antigorite

Gian Carlo Capitani,[1,*] Lars Stixrude,[2] and Marcello Mellini[3]

[1]Dipartimento di Scienze Geologiche e Geotecnologie, Università di Milano Bicocca, Piazza della Scienza 4, 20126 Milano, Italy
[2]Department of Earth Sciences, University College London, Gower Street, London WC1E 6BT, U.K.
[3]Dipartimento di Scienze della Terra, Università di Siena, Via Laterina 8, 53100 Siena, Italy

Abstract

We have investigated the antigorite $m = 17$ structure [$Mg_{48}Si_{34}O_{85}(OH)_{62}$] by density functional theory (DFT), with the aim to probe the method on such a large and low symmetry (*Pm*) system. We found a satisfactory match with the experiments using both LDA and GGA approximations to exchange-correlation, although the former performs slightly better here. Predicted cell constants are within 0.3% for LDA, and 0.5% for GGA, of the experimental values. Average atomic displacements after relaxation are within ~0.06 Å. All the fine structural details of antigorite are reproduced: apical Si-O bonds shorter than basal Si-O bonds; external Mg-O distances shorter than internal Mg-O distances; pronounced tetrahedral ditrigonal distortion. Where palpably biased bond distances were present in the experimental data because of disorder, theoretical methods promptly recover the structure into more reliable bond geometry. These findings let one envisage the employment of DFT calculations as a promising tool for refining or validating complex structures, whenever the experiments suffer of limitations due to the poor quality of the material being investigated.

As an additional benefit, we also compare the total energies of two competing models for the $m = 17$ antigorite structure, the one refined by Capitani and Mellini (2004) and that proposed by Dódony et al. (2002). We found the former more stable, both as published ($\Delta E = 1.1$ kJ/mol·atom^{-1}) and after full cell relaxation at constant volume ($\Delta E = 0.5$ kJ/mol·atom^{-1}).

Keywords: Antigorite, DFT, LDA, GGA

Introduction

The serpentine mineral antigorite—$Mg_{3m-3}Si_{2m}O_{5m}(OH)_{4m-6}$, m being the number of silicate tetrahedra along a wave projecting down [010]—usually occurs in prograde metamorphic serpentinites, both under regional (e.g., Auzende et al. 2002, 2006; Padrón-Navarta et al. 2008) and contact (Mellini et al. 1987) regimes. It has also been found in altered oceanic lithosphere (Grobéty 2003; Ribeiro da Costa et al. 2008), and hydrothermal veins (Viti and Mellini 1996). Antigorite is believed able to survive to 200 km depth in subducting oceanic lithosphere (Ulmer and Trommsdorff 1995), and several phenomena are connected to its breakdown. Embrittlement due to dehydration of antigorite has been proposed as a cause of intermediate earthquakes in double seismic zones (Peacock 2001; Yamasaki and Seno 2003). The water released upon antigorite breakdown would cause calc-alkaline volcanism at convergent margins (Ulmer and Trommsdorff 1995; Kawakatsu and Watada 2007) and serpentinization of the forearc mantle wedge (Hyndman and Peacock 2003; Bostock et al. 2002). An understanding of the role of antigorite in the geologic processes associated with these settings, and inferences of its presence by remote methods such as seismic imaging, require a detailed understanding of its complex structure and its physical properties.

The structure of natural and synthetic antigorite is difficult to determine in the lab. Antigorite specimens, when imaged with a transmission electron microscope, appear highly faulted, thus preventing or highly complicating any further structural analysis. Even in the most fortunate cases, crystal disorder (mainly as *b*/3 stacking disorder or polysomatic disorder) must be taken into account and modeled to achieve reliable structural data (Capitani and Mellini 2004, 2006). This is a general problem not limited to serpentine, and typical of many poorly crystalline, fine-grained materials. Whenever the samples are not ordered at a scale suitable for single-crystal structural analysis, one typically uses X-ray powder diffraction and/or electron crystallography. Unfortunately, these methods also have limitations, since the former suffers from an unfavorable ratio of the number of data to the number of structural parameters to be determined, and the latter from problems related to dynamical scattering.

In part because of these difficulties, two competing and mutually exclusive models have been proposed by Capitani and Mellini (2004, 2006) and Dódony et al. (2002, 2006). To further discriminate between these two models, we now take an entirely different approach based on density functional theory. We use first-principles calculations to further explore the crystal chemistry of these two models and to test their relative energetic favorability. A similar approach was taken by Stixrude and Peacor (2002) in an investigation of competing structure models of illite-smectite. We further show how density functional theory can be used systematically to improve proposed structures based on experimental data, an approach that has been used in other systems (e.g., Weirich 2003).

* E-mail: giancarlo.capitani@unimib.it

Structural models

The crystal structure of the antigorite $m = 17$ polysome was solved by Capitani and Mellini (2004) using single-crystal X-ray diffraction and direct methods. The structure model was refined to an *R*-index on observed reflections of 0.058. The structure (Fig. 1a) consists of a continuous, wavy O-sheet with Mg atoms in octahedral coordination, and a T-sheet (6-membered silicate tetrahedral rings) that links to the O-sheet on the concave side, switching polarity every half-wave at the flex lines (reversals). At reversal lines the T-sheet exhibits two different types of local structures: 8-reversals [8-membered tetrahedral rings alternating with 4-membered tetrahedral rings—a structural feature also present in previous models by Zussman (1954), Kunze (1956, 1958), and Uehara (1998)] and 6-reversals (6-membered tetrahedral rings with local TOT configuration). Overall, the structure has *Pm* symmetry with cell constants: $a = 43.505$, $b = 9.251$, $c = 7.263$ Å, $\beta = 91.32°$, and 194 atoms in the asymmetric unit (291 in the cell).

During refinement, structural disorder was modeled to achieve convergence. In fact, Fourier synthesis maps revealed two types of residues, which were interpreted to be due to *b*/3 stacking disorder [i.e., *b*/3 sliding of the tetrahedral sheet on the (001) plane] and polysomatic disorder (i.e., wavelength variation), respectively. The latter has its major negative influence in the tetrahedral sheet, at reversal lines. Here a given polysome, say $m = 17$, may transform, for instance, to an $m = 18$, simply by switching polarity of few tetrahedra. Only a few Si-O bonds need to be broken and only a few need to be established, without any major structural rearrangement in either the remaining part of the tetrahedral sheet or the entire octahedral sheet (Fig. 1b). Because of polysomatic disorder, few Si-O bonds at tetrahedral reversals may produce unreliable long distances (see Table 1).

In an earlier paper Dódony et al. (2002), after HRTEM investigation, had suggested another model for antigorite, differing from that of Capitani and Mellini (2004, 2006) by the absence of the 8-reversal in the tetrahedral sheet—all the rings possessing roughly equal hexagonal configuration like in lizardite—and by the presence of octahedral offsets at local 2_1-axes. The coordination number of the Mg atoms along these offsets is still six, but oxygen atoms form three-sided prisms (see below). Also the curvatures of the half-waves are much more pronounced in this model with respect to the Capitani and Mellini (2004, 2006) model. Overall, the structure is triclinic with *P*1 symmetry.

Computational method

We performed first-principles quantum mechanical calculations based on density functional theory (DFT) (Hohenberg and Kohn 1964; Kohn and Sham 1965). While the theory is exact, the exact form of the exchange-correlation functional is unknown and must be approximated. We investigate two widely used approximations: the local density approximation (LDA), and the more recently developed generalized gradient approximation (GGA) (Lundqvist and March 1987; Perdew et al. 1996). While LDA appears to give superior results for the structure and physical properties of silicates including phyllosilicates (Stixrude 2002; Fumagalli and Stixrude 2007; Mookherjee and Stixrude 2009), there is some evidence that GGA yields superior results for energetics (Yu et al. 2008), and for some hydrogen-bonded systems (Tsuchiya et al. 2008); LDA and GGA appear to bracket the correct energetics (Yu et al. 2008). Other functionals that

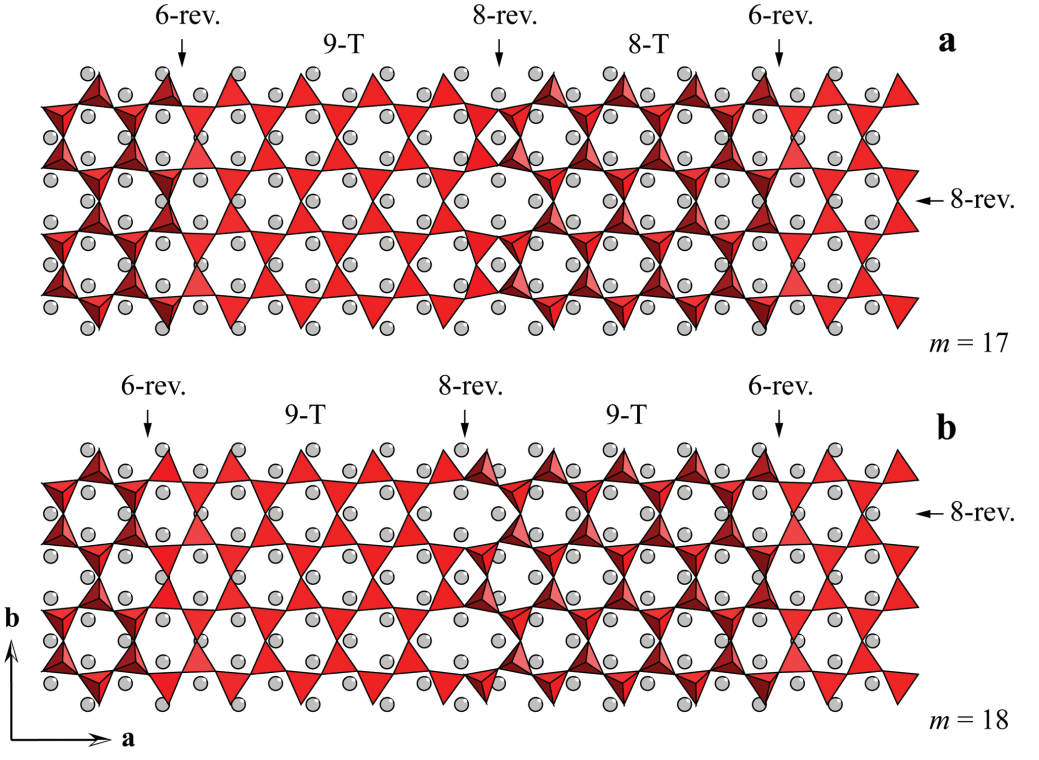

Figure 1. Drawing showing the mechanism by which an $m = 17$ antigorite polysome (**a**) transforms to an $m = 18$ polysome (**b**), simply by flipping of a few tetrahedra at reversal positions. Note how the 6-reversal and the 8-reversal positions are shifted along *x* and along *y*. The underlying octahedral sheet (only Mg atoms are indicated by gray circles), as well as the rest of the tetrahedral sheet, remain unaffected by polysomatic disorder. Note: color online.

TABLE 1. Comparison among cell constants and bond lengths (standard deviations in parentheses) as published (unrelaxed) and after structural relaxation (LDA, GGA)

	Capitani and Mellini (2004)						Dódony et al. (2002)			
	Unrelaxed*		LDA		GGA		Unrelaxed†		LDA	
a (Å)	43.5050		43.4049		43.5974		43.500		43.633	
b	9.2509		9.2428		9.2786		9.230		9.205	
c	7.2625		7.2858		7.2255		7.270		7.268	
α (°)	90.000		90.000		90.000		90.00		88.37	
β	91.316		91.170		91.124		92.00		91.70	
γ	90.000		90.000		90.000		84.75		84.92	
<Mg-O> (Å)	2.088	(47)	2.085	(53)	2.099	(53)	2.091	(74)	2.087	(80)
Max	2.207		2.224		2.221		2.421		2.859	
Min	2.005		2.018		2.027		1.775		1.980	
<Mg-O_{ext}>	2.047	(24)	2.038	(11)	2.049	(12)	–		–	
<Mg-O_{int}>	2.123	(29)	2.127	(38)	2.142	(32)	–		–	
<Si-O> (Å)	1.637	(37)	1.627	(20)	1.636	(21)	1.626	(22)	1.626	(21)
Max	1.795		1.649		1.660		1.747		1.662	
Min	1.553		1.593		1.600		1.576		1.588	
<Si-O_A>	1.620	(36)	1.596	(4)	1.603	(4)	–		–	
<Si-O_B>	1.642	(35)	1.637	(10)	1.647	(12)	–		–	
<O-H> (Å)	*0.999*	*(12)*	0.979	(2)	0.972	(2)	*1.000*		0.979	(3)
Max	*1.029*		0.983		0.976		*1.000*		0.985	
Min	*0.962*		0.975		0.969		*1.000*		0.975	
<O-H_{ext}>	*0.996*	*(14)*	0.980	(1)	0.973	(1)	–		–	
<O-H_{int}>	*1.003*	*(7)*	0.976	(1)	0.970	(1)	–		–	
Mg16-Mg35	–		–		–		2.744		2.992	
Mg19-Mg39	–		–		–		2.753		2.993	
Mg20-Mg38	–		–		–		2.753		2.987	

* O-H bonds in italics to emphasize that the hydrogen *z* coordinates were refined with restraints, while *x* and *y* were constrained to the bonded O atoms.
† O-H bonds in italics to emphasize that H atoms were put in calculated positions, since missing in the published data.

include some component of exact Hartree-Fock exchange may yield superior results for some systems (Prencipe and Nestola 2005), but have not yet been tested on phyllosilicates.

To make the solution tractable, one other essential approximation is the pseudopotential approximation (Heine 1970). This approximation is physically motivated by the argument that the core electrons participate little in bonding and structural changes. The nucleus and core electrons are replaced by a simpler object, the pseudopotential, which has the same scattering properties. We used ultrasoft Vanderbilt (Vanderbilt 1990; Kresse et al. 1992) pseudopotentials, which limit the size of the plane-wave basis set required to accurately represent charge density and potential.

All computations were performed with the plane-wave pseudopotential method in the Vienna ab initio simulation package (VASP) (Kresse and Hafner 1993; Kresse and Furthmüller 1996a, 1996b). Calculated forces and stresses are used to perform complete structural relaxations at constant volume via a conjugate gradient scheme that systematically modifies the structure until net forces and deviatoric stresses fall below a tolerance threshold. The relaxation scheme is based on the method of Wentzcovitch (1991) and Wentzcovitch et al. (1993), which conserves the space group symmetry.

Total static energy calculations were performed either in the absence of relaxation or allowing relaxation. The crystal structures of the $m = 17$ polysome by Capitani and Mellini (2004) and by Dódony et al. (2002), expressed in their respective primitive *P*1 unit cells [291 atoms for a $Mg_{48}Si_{34}O_{85}(OH)_{62}$ unit formula][1], were used, as published in the absence of relaxation, and as an initial guess in the presence of relaxation. We used an energy cutoff of 500 eV, and a Monkhorst-Pack (Monkhorst and Pack 1976) 1 × 2 × 2 k point mesh, yielding a value of the energy difference between the two structures that is converged to better than 0.1 meV/unit cell.

[1]Dódony et al. (2002) did not give hydrogen coordinates in their published tables. For the sake of consistency, H atoms were added in calculated positions with the same *x* and *y* coordinates as the linked oxygen atoms, and 1 Å distant along *z* from the latter.

RESULTS

Structural relaxation of antigorite $m = 17$

The resulting cell constants and average bond distances after structural relaxation with LDA and GGA potentials are compared with the experimental results for the Capitani and Mellini (2004) structure in Table 1. LDA calculations slightly underestimate the *a* and *b* parameters and overestimate *c* with respect to the experimental values. GGA calculations slightly overestimate *a*, but substantially overestimate *b* and underestimate *c*. The monoclinic β angle is slightly reduced compared with experiment in both cases. As far as cell constants are concerned, LDA values better match experiments, the agreement being within 0.3% for LDA and within 0.5% for GGA. The good agreement between LDA and experiment is further supported by the calculated pressure: –2.67 GPa, which is very similar to that expected at static conditions based on experimental results (Mookherjee and Stixrude 2009). GGA on the other hand, predicts a positive static pressure (2.18 GPa) that is much larger than that expected at static conditions.

Theoretical structural relaxations yield structures that are more sensible crystal-chemically relative to those originally determined experimentally (Table 1). Whereas the octahedral sheet is not significantly affected by relaxation, especially using LDA, the tetrahedral sheet appears modified. The Si-O bonds are less dispersed after relaxation and no longer show the anomalous long and short distances present in the experimental tetrahedral sheet. Capitani and Mellini (2004) interpreted these sporadic anomalous distances, located at tetrahedral reversals, as biased due to polysomatic disorder. Because of disorder, electron

density at reversals is delocalized over several sites and the scattering power affected consequently, which in turn yields poorly constrained bond geometry. In contrast, the octahedral sheet is basically unaffected by polysomatic (and stacking) disorder, and this explains why the relaxed octahedral sheet closely matches the refined one.

The fine structural details of antigorite are well reproduced: apical Si-O_A bonds are shorter than basal Si-O_B bonds (LDA: 1.596 vs. 1.637 Å; GGA: 1.603 vs. 1.647 Å); external Mg-O_{ext} distances are shorter than internal Mg-O_{int} distances (LDA: 2.038 vs. 2.127 Å; GGA: 2.049 vs. 2.142 Å).

Also the O-H bonds are less dispersed in the relaxed structure. However, in this case, comparison is difficult because of the very limited scattering power of H atoms. During X-ray refinement, the *x* and *y* hydrogen coordinates were assumed to be identical to those of the bonded O atoms and the O-H distances were restrained to a fixed value. Therefore, the present simulations most probably represent the best estimate of hydrogen distributions within antigorite (Fig. 2). The theoretically relaxed structure reveals a significant difference between the lengths of internal O-H_{int} distances (LDA: 0.976 Å; GGA: 0.970 Å) and external O-H_{ext} distances (LDA: 0.980 Å; GGA: 0.973 Å), a distinction that is not resolvable with XRD data alone.[2]

The mean atomic displacements during relaxation are ~0.06 Å along *x*, ~0.02 Å along *y*, and ~0.04 Å along *z* (Table 2). In terms of fractional coordinates, the major displacement occurs along *z* (~0.5%), then along *y* (~0.2%), and along *x* (~0.1%). The largest readjustments involve, in most cases, the basal O atoms, and in particular the B17 oxygen, located at the 6-reversal (Fig. 1) and affected by polysomatic disorder. Finally (and not surprisingly), the Mg atoms move on average less than Si atoms; the latter, in turn, move less than O atoms, which move less than H atoms. This feature in part reflects the relative scattering power of these elements, and in part the fact that magnesium atoms in the octahedral sheet of antigorite are almost insensitive to stack-

[2]Deposit item AM-09-041, LDA relaxed atomic coordinates of all the atomic specie. Deposit items are available two ways: For a paper copy contact the Business Office of the Mineralogical Society of America (see inside front cover of recent issue) for price information. For an electronic copy visit the MSA web site at http://www.minsocam.org, go to the American Mineralogist Contents, find the table of contents for the specific volume/issue wanted, and then click on the deposit link there.

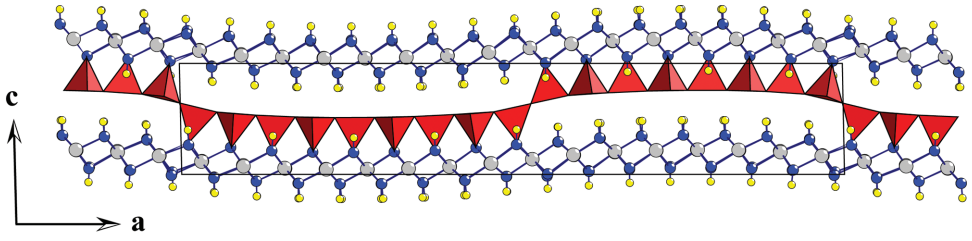

FIGURE 2. Antigorite $m = 17$ structure as seen along [010] after relaxation (LDA potentials) showing SiO_4 tetrahedra (red), Mg atoms (gray), O atoms (blue), and H atoms (yellow) in their optimized positions. Note: color online.

TABLE 2. Average and maximum displacements (Å) of the atomic coordinates in the relaxed structures (LDA, GGA) with respect the unrelaxed, as published structures

	Capitani and Mellini (2004)						Dódony et al. (2002)		
	LDA			GGA			LDA		
	Δ*x*	Δ*y*	Δ*z*	Δ*x*	Δ*y*	Δ*z*	Δ*x*	Δ*y*	Δ*z*
Mean	0.05940	0.01989	0.03549	0.05135	0.02386	0.03839	0.09288	0.15117	0.29918
Max	0.18212	0.12809	0.29046	0.28764	0.13748	0.23965	0.42007	0.64773	0.50075
<M>	0.04530	0.00640	0.01356	0.05162	0.01266	0.02423	0.06479	0.18198	0.29516
Max	0.11740	0.02268	0.08205	0.09748	0.03649	0.10760	0.15001	0.64773	0.46853
<T>	0.05196	0.00887	0.02442	0.04976	0.01597	0.03277	0.08080	0.09007	0.27216
Max	0.11429	0.02204	0.05118	0.09061	0.04037	0.06202	0.27321	0.19553	0.46073
<O>	0.06007	0.01723	0.03785	0.05294	0.02240	0.04664	0.09205	0.14442	0.29707
Max	0.15004	0.12809	0.29046	0.28764	0.13748	0.23965	0.27430	0.63620	0.49361
<A>	0.06516	0.01281	0.03344	0.04163	0.01915	0.03941	–	–	–
Max	0.11309	0.05888	0.10727	0.08200	0.05420	0.09871	–	–	–
<B>	0.06408	0.03251	0.04445	0.07246	0.03865	0.06343	–	–	–
Max	0.15004	0.12809	0.29046	0.28764	0.13748	0.23965	–	–	–
<W>	0.05695	0.00896	0.03018	0.03898	0.01213	0.04011	–	–	–
Max	0.12786	0.02853	0.10392	0.09549	0.03486	0.10770	–	–	–
<V>	0.04616	0.00216	0.04720	0.05395	0.00730	0.02802	–	–	–
Max	0.08459	0.00409	0.15196	0.13581	0.01379	0.12322	–	–	–
<OH>	0.07277	0.04269	0.05296	0.04824	0.04034	0.03286	0.12323	0.17685	0.32213
Max	0.18212	0.11911	0.20194	0.16010	0.12886	0.11904	0.42007	0.60835	0.50075
<H>	0.07182	0.05774	0.04168	0.04742	0.05192	0.02770	–	–	–
Max	0.18212	0.11911	0.12304	0.13411	0.12886	0.07350	–	–	–
<I>	0.07167	0.00216	0.08205	0.05297	0.00730	0.04497	–	–	–
Max	0.16555	0.00409	0.20194	0.16010	0.01379	0.11904	–	–	–

Notes: M = octahedral sites; T = tetrahedral sites; O = oxygen sites; A = tetrahedral apical oxygen sites; B = tetrahedral basal oxygen sites; W = octahedral external oxygen sites; V = octahedral internal oxygen sites; OH = hydrogen sites; H = external hydrogen sites; I = internal hydrogen sites.

TABLE 3. Average thickness (Å) of the octahedral (M) and tetrahedral (T) sheets and average distances (Å) of the octahedral cation from the plane of the external (M⊥W) and internal (M⊥V) oxygen atoms for the Capitani and Mellini (2004) structure

	XRD		LDA		GGA	
<M>	2.111	(32)	2.106	(18)	2.134	(15)
Max	2.162		2.166		2.182	
Min	2.061		2.089		2.119	
<M⊥W>	0.956	(23)	0.958	(36)	0.966	(34)
Max	0.989		1.085		1.091	
Min	0.901		0.930		0.938	
<M⊥V>	1.151	(24)	1.149	(21)	1.168	
Max	1.216		1.161		1.182	(23)
Min	1.106		1.081		1.091	
<T>	2.244	(69)	2.212	(19)	2.228	(18)
Max	2.456		2.251		2.267	
Min	2.162		2.199		2.214	

Note: Comparison among experimental (XRD) and calculated values (LDA and GGA).

ing and polysomatic disorder, and thus much more constrained than any other atom.

Octahedral thicknesses in the relaxed structures are more uniform than in the experimental one (Table 3). LDA calculations better reproduce the experimental results. As in the refined structure, the Mg cations are displaced toward the external hydroxyls to satisfy local charge balance. Because of disorder in the tetrahedral sheet, it is difficult to say if the thickness of the tetrahedral sheet is underestimated in the relaxed structures with respect to the experimental one (in LDA more than in the GGA), or vice versa. As regards O-O distances in the interlayer (Table 4), LDA seems to overestimate such distances with respect to the experimental values and GGA to underestimate them, in keeping with the observed variations of the *c* parameter. These anomalies may be due either to (1) lack of a thermal contribution to the structural relaxation in these static (0 K) calculations, or (2) the inability of the LDA and GGA to capture the physics of the weak dispersion interactions in the interlayer (Thonhauser et al. 2007).

Ditrigonal distortions of the tetrahedral rings (Table 5) are on average larger in the relaxed structure than in the experimental structure, moreso in the case of GGA than LDA, consistent with the GGA results on lizardite by Balan et al. (2002). Finally, the radii of curvature and the aperture angles of the two half-waves (Table 6) are more similar to each other in the relaxed structures than in the experimental structure. In other words, the half-wave asymmetry is reduced in the relaxed structure, in LDA moreso than in GGA calculations.

Energetics of antigorite *m* = 17

Table 7 reports the total static energies of the two competing models, as published (no relaxation) and after relaxation of cell constants and atomic coordinates. Without relaxation, according to LDA potentials the Capitani and Mellini (2004) model possesses a total energy that is 3.34 eV/unit cell (11.5 meV·atom^{-1}) lower than that of the Dódony et al. (2002) model. After relaxation, the difference reduces to 1.58 eV (5.4 meV·atom^{-1}). GGA potentials give similar results (6.8 meV·atom^{-1}). The difference in internal energy $\Delta E(V_X)$ at the experimental volume V_X that we have computed is very similar to the difference in Gibbs free energy at zero pressure, $\Delta G(0) \approx \Delta E(V_X) + V_X\Delta(P_X^2)/(2K)$, where P_X is the DFT pressure at V_X and K is the bulk modulus, which we take from the static results of Mookherjee and Stixrude (2009). The magnitude of the correction term is 0.7 meV·atom^{-1}, a small fraction of $\Delta E(V_X)$.

To understand the origin of the significant energy difference (as well as its reduction after relaxation), we analyzed the bond geometries of the Dódony et al. (2002) structure before and after relaxation (Table 1). Both Mg-O bonds and Si-O bonds show some anomalous values, either too short (Mg-O_{MIN} = 1.775; Si-O_{MIN} = 1.576 Å) or too long (Mg-O_{MAX} = 2.421; Si-O_{MAX} =

TABLE 4. Average, maximum, and minimum distances (Å) between the tetrahedral basal O atoms and the closer external octahedral O atoms

	XRD		LDA		GGA	
<B-W>	3.092	(131)	3.126	(138)	3.069	(173)
Max	3.421		3.457		3.500	
Min	2.860		2.968		2.905	
<B-W>$_L$	3.087	(147)	3.141	(141)	3.083	(170)
Max	3.421		3.433		3.441	
Min	2.860		2.968		2.905	
<B-W>$_S$	3.098	(113)	3.142	(141)	3.092	(182)
Max	3.350		3.457		3.500	
Min	2.920		2.970		2.905	

Notes: Comparison among experimental (XRD) and calculated values (LDA and GGA) for the Capitani and Mellini (2004) structure. Data for the long (L) and the short (S) half-wave only are also reported.

TABLE 5. Average, maximum, and minimum ditrigonal distortion α angles (°) of the tetrahedral rings for the Capitani and Mellini (2004) structure

	XRD	LDA	GGA
<α>	7.41	10.90	12.01
Max	13.63	15.12	16.13
Min	3.53	7.30	8.49
<α>$_L$	8.83	10.49	11.62
Max	13.63	14.78	15.19
Min	6.97	8.56	9.92
<α>$_S$	6.00	11.31	12.39
Max	9.38	15.12	16.13
Min	3.53	7.30	8.49
6-rev.	5.95	7.14	8.40
8-rev.	13.85	13.54	14.02
4-rev.	13.30	10.76	11.32

Notes: Comparison among experimental (XRD) and calculated values (LDA and GGA). Values pertinent to only the long (L) and the short (S) half-waves are also reported. α is defined as the average deviation from 120°. Analogous distortion parameters, defined as the average deviation from 90 and 135°, are given for the 8-membered ring (8-rev.) and the 4-membered ring (4-rev.), respectively.

TABLE 6. Relevant half-wave parameters

	Capitani and Mellini (2004)			Dódony et al. (2002)	
	Unrelaxed	LDA	GGA	Unrelaxed	LDA
d_S (Å)	20.462	20.376	20.448	20.5	20.6
R_S (Å)	110.5	105.8	106.7	46.2	75.4
ρ_S (°)	10.6	11.1	11.0	25.8	15.7
d_L (Å)	23.045	23.029	23.149	23.0	23.0
R_L (Å)	99.4	105.9	111.5	46.2	74.2
ρ_L (°)	13.3	12.5	11.9	28.9	17.9

Notes: Comparison among as published (unrelaxed) and calculated values (LDA, GGA). d = length of the half-wave; R = radius of curvature; ρ = aperture angle; (L = long half-wave; S = short half-wave).

TABLE 7. Total energy (eV/atom) of the two competing *m* = 17 antigorite structure models investigated

	Capitani and Mellini (2004)	Dódony et al. (2002)
Unrelaxed	–6.963234	–6.951747
LDA	–6.983189	–6.977770
GGA	–6.435414	–6.428606

1.747 Å), which are located at local 2_1-axes at 6-reversals where octahedral offsets occur. After relaxation the Si-O bonds show normal values, but the Mg-O bonds still show anomalous values, although shifted toward higher minimum and maximum values (1.980 and 2.859 Å, respectively). Even more significant is the behavior of Mg-Mg distances at local 2_1-axes at 6-reversals. In the unrelaxed structure these two cations are too close (2.744–2.753 Å); therefore, they are forced to move away from each other during relaxation (2.987–2.992 Å) to minimize the repulsive energy (Fig. 3), destroying the local 2_1-axis operator. Overall, the original three-sided prisms (Fig. 4a) are forced to progressively change into a more stable, though still distorted, octahedral configuration (Fig. 4b). It thus appears that the octahedral offsets at local 2_1-axes at 6-reversals with Mg atoms at the center of triangular prisms are highly unstable structural configurations that accumulate most of the energy excess.

On average, the atomic displacements after relaxation from the Dódony et al. (2002) structure are at least one order of magnitude larger than those from the m = 17 structure of Capitani and Mellini (2004) (Table 2). The larger average displacements along y reflect, in part, the recovery of the anomalous bond geometry discussed above; and in part from the increase of the tetrahedral ring distortion (ditrigonalization) apparent in Figure 2. The large displacements along z reflect flattening of the half-waves in the relaxed structure relative to the unrelaxed structure, as shown by the values of the radii of curvature (74.2–75.4 vs. 46.2 Å) and of the aperture angles (15.7–17.9 vs. 25.8–28.9), respectively (Table 6). Relaxation thus pushes the structure toward normal octahedral configuration of the Mg atoms and flat half-waves, i.e., toward something resembling the Capitani and Mellini (2004) structure.

Concluding remarks

The antigorite structure is characterized by half-waves and reversals of the T-O sheets. At these reversals, the standard geometry of T sheets and O sheets cannot both be preserved. Two competing solutions have been proposed based on experimental data: 8-reversals, that is the formation of 8-membered rings of SiO_4 tetrahedra, with no octahedral offsets (Capitani and Mellini 2004), and the formation of MgO_6 ditrigonal prisms, with only 6-membered tetrahedral rings (Dódony et al. 2002).

Single-crystal X-ray diffraction structure refinements unequivocally support the model of Capitani and Mellini (2004). These data were collected on the most ordered antigorite sample known to date, and the quality of the inversion is high ($R_{4\sigma}$ = 0.0577). We believe that disagreement in the interpretation of HRTEM and SAED images arises fundamentally because, unlike single-crystal X-ray diffraction, there is no reliable procedure for the formal inversion of intensities (Capitani and Mellini 2008). Electron diffraction can be a powerful tool to rule out structural models, but its ability to uniquely solve structures is limited. We have demonstrated the limitations caused by multiple scattering of the reciprocal lattice sectioning method used by Dódony et al. (2006) and shown that the structure of Capitani and Mellini (2004) is in fact consistent with HRTEM and SAED images (Capitani and Mellini 2008).

The theoretical results presented here fully support the structural model of Capitani and Mellini (2004). The energy difference between the two models is large before (11.5 meV/atom or 1.1 kJ/mol·atom^{-1}) and after relaxation (5.4 meV/atom or 0.5 kJ/mol·atom^{-1}). For comparison, the difference in enthalpy of formation at ambient conditions from quartz and cristobalite is 1.0 kJ/mol·atom^{-1}, and that from andalusite and sillimanite is 0.4 kJ/mol·atom^{-1} (Waldbraum 1965).

The energy difference between the two structural models can

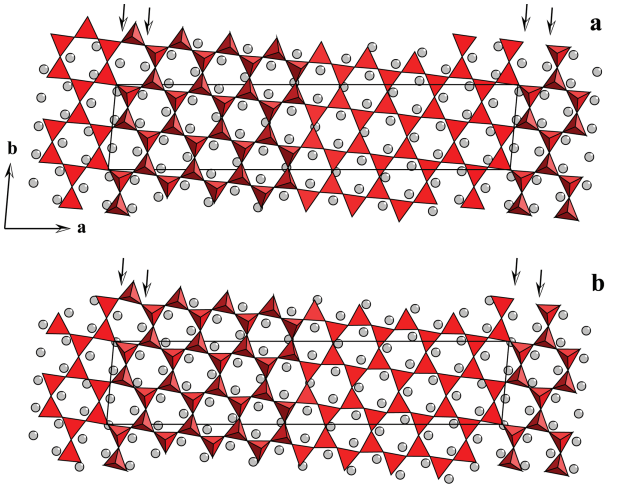

Figure 3. Comparison between the Dódony et al. (2002) model for antigorite m = 17 as published (**a**) and after relaxation (**b**). Note the relative displacements of the Mg sites (arrows) at the 2_1-axis 6-reversal.

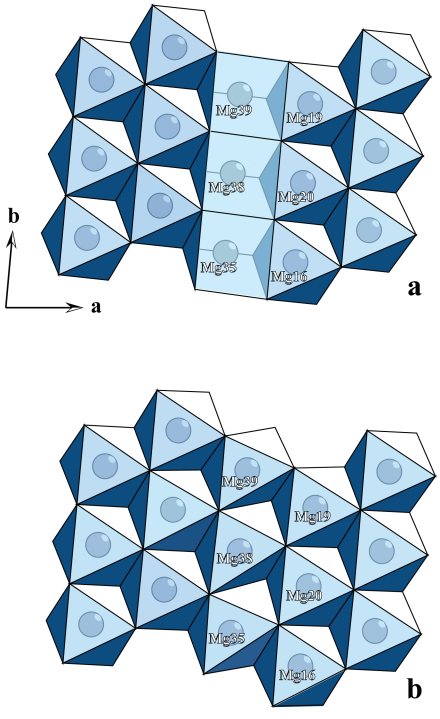

Figure 4. Comparison of the Mg coordination polyhedra in the Dódony et al. (2002) model, before (**a**) and after relaxation (**b**). Note how the coordination polyhedra transform from three-sided prisms to distorted octahedra.

be attributed primarily to the presence of highly unfavorable MgO_6 ditrigonal prisms in the model of Dódony et al. (2002). Such Mg-coordination environments are not known in other silicates. The DFT relaxations modify the geometry of these coordination environments substantially, but within the constraints of the bond geometry of the Dódony et al. (2002) model still yield a highly distorted octahedron. In contrast, the 4- and 8-membered rings of the structure of Capitani and Mellini (2004) are common in a wide variety of silicates (Stixrude and Bukowinski 1990). DFT relaxations alter the X-ray refined structure only slightly and yield bond geometries and coordination environments that lie well within the range known from other silicates. We find that the computed powder X-ray diffraction patterns of the LDA and GGA relaxed structures are almost indistinguishable from that of the experimentally refined structure, whereas the structure of Dódony et al. (2002) differs substantially (Fig. 5).

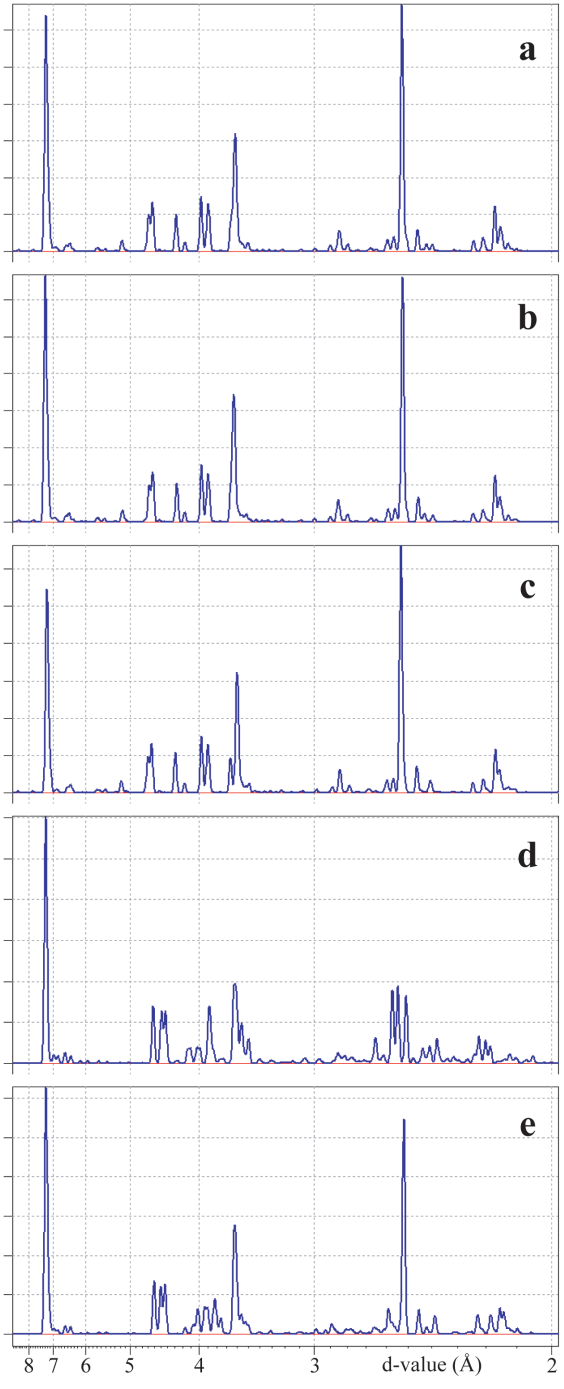

FIGURE 5. Comparison among simulated XRPD patterns. Capitani and Mellini (2004) structure: (**a**) experimental refined structure; (**b**) LDA relaxed structure; (**c**) GGA relaxed structure. Dódony et al. (2002) structure: (**d**) published structure; (**e**) LDA relaxed structure.

First-principles calculations may become an important tool of structure determination. This may be particularly true for large or complex structures, which are now accessible to density functional theory. Within both LDA and GGA, the slight biases present in the solution of Capitani and Mellini (2004) due to the presence of locally disordered sites promptly relax to values that are more sensible crystal-chemically. We have shown how DFT may also be used to locate weak scatterers such as H atoms in complex structures. DFT calculations may be particularly useful whenever experimental data are affected by limitations of sample quality or geometry, for example in powder X-ray diffraction or because of sample disorder, or in techniques such as electron crystallography where multiple scattering hinders unique solutions.

ACKNOWLEDGMENTS

This work was possible thanks to a grant for computer time at the Caspur HPC facilities to G.C.C. Luca Ferraro is greatly acknowledged for computer help with the "Poseidon" AMD Opteron Cluster. Comments by Mauro Prencipe and an anonymous referee greatly improved the manuscript.

REFERENCES CITED

Auzende, A., Devouard, B., Guillot, S., Daniel, I., Baronnet, A., and Lardeaux, J.M. (2002) Serpentinites from Central Cuba: petrology and HRTEM study. European Journal of Mineralogy, 14, 905–914.

Auzende, A., Guillot, S., Devouard, B., and Baronnet, A. (2006) Serpentinites in an Alpine convergent setting: effects of metamorphic grade and deformation on microstructures. European Journal of Mineralogy, 18, 21–33.

Balan, E., Saitta, A.M., Mauri, F., Lemaire, C., and Guyot, F. (2002) First-principles calculation of the infrared spectrum of lizardite. American Mineralogist, 87, 1286–1290.

Bostock, M.G., Hyndman, R.D., Rondenay, S., and Peacock, S.M. (2002) An inverted continental Moho and serpentinization of the forearc mantle. Nature, 417, 536–538.

Capitani, G.C. and Mellini, M. (2004) The modulated crystal structure of antigorite: the m = 17 polysome. American Mineralogist, 89, 147–158.

——— (2006) The crystal structure of a second antigorite polysome (m = 16), by single crystal synchrotron diffraction. American Mineralogist, 91, 394–399.

——— (2008) Rationale for the existence of 4- and 8-reversals in antigorite. American Mineralogist, 93, 796–799.

Dódony, I., Pósfai, M., and Buseck, P.R. (2002) Revised structure models for antigorite: An HRTEM study. American Mineralogist, 87, 1443–1457.

——— (2006) Does antigorite really contain 4- and 8-membered rings of tetrahedra? American Mineralogist, 91, 1831–1838.

Fumagalli, P. and Stixrude, L. (2007) The 10 Å phase at high pressure by first principles calculations and implications for the petrology of subduction zones. Earth and Planetary Science Letters, 260, 212–226.

Grobéty, B. (2003) Polytypes and higher-order structures of antigorite: a TEM study. American Mineralogist, 88, 27–36.

Heine, V. (1970) The pseudopotential concept. Solid State Physics, 24, 1–37.

Hohenberg, P. and Kohn, W. (1964) Inhomogeneous electron gas. Physical Review B, 136, 864–871.

Hyndman, R.D. and Peacock, S.M. (2003) Serpentinization of the forearc mantle. Earth and Planetary Science Letters, 212, 417–432.

Kawakatsu, H. and Watada, S. (2007) Seismic evidence for deep-water transportation in the mantle. Science, 316, 1468–1471.

Kohn, W. and Sham, L.J. (1965) Self-consistent equations including exchange and correlation effects. Physical Review A, 140, 1133–1138.

Kresse, G. and Furthmüller, J. (1996a) Efficiency of ab-initio total energy calculations for metals and semiconductors. Computational Material Science, 6, 15–50.

——— (1996b) Efficient iterative schemes for *ab initio* total-energy calculations using a plane-wave basis set. Physical Review B, 54, 11169–11186.

Kresse, G. and Hafner, J. (1993) *Ab initio* molecular-dynamics for liquid-metals. Physical Review B, 47, 558–561.

Kresse, G., Hafner, J., and Needs, R.J. (1992) Optimized norm-conserving pseudopotentials. Journal of Physics, Condensed Matter, 4, 7451–7468.

Kunze, V.G. (1956) Die gewellte struktur des antigorits, I. Zeitschrift für Kristallographie, 108, 82–107.

——— (1958) Die gewellte struktur des antigorits, II. Zeitschrift für Kristallographie, 110, 282–320.

Lundqvist, S. and March, N.H. (1987) Theory of the Inhomogeneous Electron Gas. Plenum, New York.

Mellini, M., Trommsdorff, V., and Compagnoni, R. (1987) Antigorite polysomatism: Behavior during progressive metamorphism. Contributions to Mineralogy and Petrology, 97, 147–155.

Mookherjee, M. and Stixrude, L. (2009) Structure and elasticity of serpentine at high pressure. Earth and Planetary Science Letters, 279, 11–19.

Monkhorst, H.J. and Pack, J.D. (1976) Special points for Brillouin-zone integrations. Physical Review B, 13, 5188–5192.

Padrón-Navarta, J.A., López Sánchez-Vizcaíno, V., Garrido, C.J., Gómez Pugnaire, M.T., Jabaloy, A., Capitani, G.C., and Mellini, M. (2008) Highly ordered antigorite from Cerro del Almirez HP-HT serpentinites, SE Spain. Contributions to Mineralogy and Petrology, 156, 679–688.

Peacock, S.M. (2001) Are the lower planes of double seismic zones caused by serpentine dehydration in subducting oceanic mantle? Geology, 29, 299–302.

Perdew, J.P., Burke, K., and Ernzerhof, M. (1996) Generalized gradient approximation made simple. Physical Review Letters, 77, 3865–3868.

Prencipe M. and Nestola F. (2005) Quantum-mechanical modeling of minerals at high pressures. The role of the Hamiltonian in a case study: the beryl ($Al_4Be_6Si_{12}O_{36}$). Physics and Chemistry of Minerals, 32, 471–479.

Ribeiro Da Costa, I., Barriga, F.J.A.S., Viti, C., Mellini, M., and Wicks, F. (2008) Antigorite in deformed serpentinites from the Mid-Atlantic Ridge. European Journal of Mineralogy, 20, 563–572.

Stixrude, L. (2002) Talc under tension and compression: Spinodal instability, elasticity, and structure. Journal of Geophysical Research, 107, 23–27.

Stixrude, L. and Bukowinski, M.S.T. (1990) Rings, topology, and the density of tectosilicates. American Mineralogist, 75, 1159–1169.

Stixrude, L. and Peacor, D.R. (2002) First-principles study of illite-smectite and implications for clay mineral systems. Nature, 420, 165–168.

Thonhauser, T., Cooper, V.R., Li, S., Puzder, A., Hyldgaard, P., and Langreth, D.C. (2007) Van der Waals density functional: Self-consistent potential and the nature of the van der Waals bond. Physical Review B, 76, 125112.

Tsuchiya, J., Tsuchiya, T., and Wentzcovitch, R.M. (2008) Vibrational properties of δ-AlOOH under pressure. American Mineralogist, 93, 477–482.

Uehara, S. (1998) TEM and XRD study of antigorite superstructures. Canadian Mineralogist, 36, 1595–1605.

Ulmer, P. and Trommsdorff, V. (1995) Serpentine stability to mantle depths and subduction related magmatism. Science, 268, 858–861.

Vanderbilt, D. (1990) Soft self-consistent pseudopotentials in a generalized eigenvalue formalism. Physical Review B, 41, 7892–7895.

Viti, C. and Mellini, M. (1996) Vein antigorites from Elba Island, Italy. European Journal of Mineralogy, 8, 423–434.

Waldbraum, D.R. (1965) Thermodynamic properties of mullite, andalusite, kyanite, and sillimanite. American Mineralogist, 50, 186–195.

Weirich, T.E. (2003) First-principles calculations as a tool for structure validation in electron crystallography. Acta Crystallographica, A60, 75–81.

Wentzcovitch, R.M. (1991) Invariant molecular dynamics approach to structural phase transitions. Physical Review B, 44, 2358–2361.

Wentzcovitch, R.M., Martins, J.L., and Price, G.D. (1993) *Ab initio* molecular dynamics with variable cell shape: Application to $MgSiO_3$. Physical Review Letters, 70, 3947–3950.

Yamasaki, T. and Seno, T. (2003) Double seismic zone and dehydration embrittlement of the subducting slab. Journal of Geophysical Research, 108, 2212–1232.

Yu, Y.G.G., Wu, Z.P., and Wentzcovitch, R.M. (2008) α–β–γ transformations in Mg_2SiO_4 in Earth's transition zone. Earth and Planetary Science Letters, 273, 115–122.

Zussman, J. (1954) Investigation of the crystal structure of antigorite. Mineralogical Magazine, 30, 498–512.

Manuscript received February 11, 2009
Manuscript accepted May 5, 2009
Manuscript handled by Artem Oganov